

Cite this: *Chem. Sci.*, 2024, 15, 12118



All publication charges for this article have been paid for by the Royal Society of Chemistry

Received 26th April 2024
Accepted 29th June 2024

DOI: 10.1039/d4sc02785j

rsc.li/chemical-science

A geminal antimony(III)/phosphorus(III) frustrated Lewis pair†

Jonas Krief, Pia C. Trapp, Yury V. Vishnevskiy,  Beate Neumann, Hans-Georg Stammer, Jan-Hendrik Lamm and Norbert W. Mitzel *

The geminal Lewis pair $(F_5C_2)_2SbCH_2P(tBu)_2$ (**1**) was prepared by reacting $(F_5C_2)_2SbCl$ with $LiCH_2P(tBu)_2$. Despite its extremely electronegative pentafluoroethyl substituents, the neutral **1** exhibits a relatively soft acidic antimony function according to the HSAB concept (hard–soft acid–base). These properties lead to a reversibility in the binding of CS_2 to **1**, as observed by VT-NMR spectroscopy, while no reaction with CO_2 is observed. The reaction behaviour towards heterocumulenes and the specific interaction situation in the CS_2 adduct were analysed by quantum chemical calculations. The FLP-type reactivity of **1** has also been demonstrated by reaction with a variety of small molecules (SO_2 , $PhNCO$, $PhNCS$, $(MePh_2P)AuCl$). The reactions of **1** with $PhNCO$ and $PhNCS$ led to different types of cyclic addition products: $PhNCO$ adds with its $N=C$ bond and $PhNCS$ adds preferentially with its $C=S$ bond. The reaction of **1** with $(MePh_2P)AuCl$ gave an adduct $\{[(F_5C_2)_2SbCH_2(tBu)_2P]_2Au\}^+$ with a clamp-like structure binding a chloride anion by its two antimony atoms in chelate mode. Compound **1** and its adducts have been characterised by X-ray diffraction experiments, multinuclear NMR spectroscopy, elemental analyses and computational calculations (DFT, QTAIM, IQA).

Introduction

Since the pioneering work of Stephan and Erker in the field of Frustrated Lewis Pairs (FLP), this part of modern main group chemistry has developed rapidly and in many directions.¹ Steric shielding and ring strain can prevent the formation of a stable adduct between Lewis acid and Lewis base sites and thus the neutralisation of the two functions within one molecule. The unused reaction potential can now be used to activate various small molecules or to catalyse reactions.^{2–5} The diversity of combinations of Lewis acids and bases in FLP systems continues to grow, but the “typical” combinations of Lewis acids of the third main group (B, Al) and Lewis bases of the fifth main group (N, P) dominate.^{6,7} The use of pnictogens in the base functions is established, but the elements of this main group can also have interesting Lewis acidic properties, making them very interesting and variable building blocks.⁸ At least since Olah’s work on the so-called magic acid, antimony compounds have become an indispensable part of Lewis acid chemistry.^{9,10} Several contributions of Gabbai and co-workers have shown that Lewis acidic stibonium ions and various stiboranes are not only able to activate C–F bonds,¹¹ but also to trap halide ions¹²

and to act as ligands for transition metal complexes.¹³ Antimony has a special position in this respect due to its most pronounced Lewis acidity within the group.¹⁴ Despite Sb(III) atoms have a free pair of electrons, their Lewis acidity can be reinforced by introducing perfluorinated substituents.^{10,15} In this way, a distinct σ -hole can be induced on the formally Lewis basic Sb(III) atom. The acidity of this σ -hole depends on the electron-withdrawing properties of the spatially opposite substituent, making it an interesting and flexible building block for the synthesis of functionalised Lewis acids and FLP systems.¹⁶

We have recently reported a bidentate and a tetradentate Sb(III)-based poly-Lewis acid capable of chelate-binding halide ions, dimethyl chalcogenides and nitrogen heterocycles by pnictogen bonding.^{17,18} We have also exploited the special properties of the $Sb(C_2F_5)_2$ moiety to develop the new neutral geminal FLP presented here. In terms of Pearson’s HSAB concept,¹⁹ the relatively soft Lewis acid Sb(III) of this unit should be favourable for reversible reactions. Similarly, we have previously introduced the Sn/P-FLP $(F_5C_2)_3SnCH_2P(tBu)_2$, which reversibly binds CO_2 while forming a stable adduct with the softer CS_2 . $(F_5C_2)_3SnCH_2P(tBu)_2$ also reacts with a variety of small molecules and stabilises highly reactive species, including the elusive sulphur monoxide.^{5,20,21}

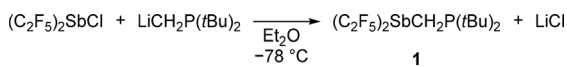
Results and discussion

Starting from $(F_5C_2)_2SbCl$,¹⁷ the intramolecular FLP $(F_5C_2)_2SbCH_2P(tBu)_2$ (**1**) was prepared by reaction with $LiCH_2P(tBu)_2$ ²² in a nucleophilic substitution (Scheme 1).

Chair of Inorganic and Structural Chemistry, Center for Molecular Materials CM₂, Faculty of Chemistry, Bielefeld University, Universitätsstraße 25, Bielefeld 33615, Germany. E-mail: mitzel@uni-bielefeld.de

† Electronic supplementary information (ESI) available. CCDC 2350371–2350377. For ESI and crystallographic data in CIF or other electronic format see DOI: <https://doi.org/10.1039/d4sc02785j>



Scheme 1 Synthesis of FLP 1 from $(F_5C_2)_2SbCl$ and $LiCH_2P(tBu)_2$.

Since **1** is a liquid under normal conditions, a single crystal suitable for X-ray diffraction was grown by *in situ* crystallisation at 283.9 K on the diffractometer. After the formation of a tiny seed crystal, the sample was cooled to 100 K. The molecular structure (Fig. 1) shows a distance between the Sb and P atoms in **1** of 3.306(1) Å, much longer than the sum of the covalent radii indicating that, at most, only a weakly stabilising interaction exists.²³ The Sb...P distance is between geminal atoms and thus by its nature less than the sum of the van der Waals radii. Therefore, the Sb–C–P angle is more telling about a possible attractive Sb...P interaction. At 110.6(1)° it is smaller than the corresponding Sn–C–P angle in the Sn/P-FLP mentioned above with 113.9(1)°. However, the Sb–C–P angle of the rigid methylene backbone is too obtuse for the formation of an intramolecular Lewis acid/base adduct, as was also observed in all $(F_5C_2)_nECH_2P(tBu)_2$ FLPs we have presented so far.^{3–5} The Sb atom is trigonal-pyramidal coordinated, as is common for trisubstituted pnictogen atoms in the oxidation state +III. Expectedly, the angles including the Sb position are between 91.3(1) and 95.8(1)°, *i.e.* close to 90°. ²⁴

The ³¹P NMR resonance of **1** at 15.5 ppm is in the typical range for methylene-bridged Lewis acid/ $P(tBu)_2$ systems (*e.g.* $\delta(^{31}P)$ $(F_5C_2)_3SnCH_2P(tBu)_2$ 17.2 ppm,⁵ $(F_5C_2)_3SiCH_2P(tBu)_2$ 18.5 ppm⁴). Also typical for these systems are the ¹³C{¹H} NMR resonances of **1** for the methylene carbon atoms at 9.0 ppm and the ¹⁹F NMR resonances of the pentafluoroethyl groups at –82.7 and –110.5/–111.1 ppm.^{4,5}

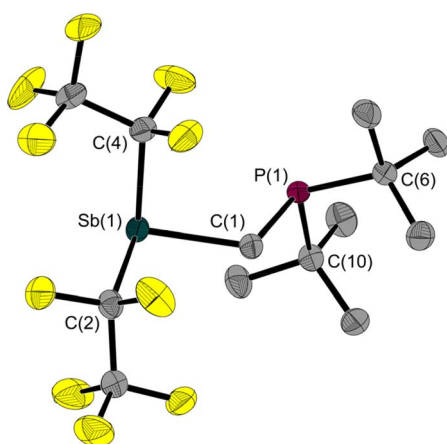


Fig. 1 Molecular structure of **1** in the solid state. Ellipsoids are set at 50% probability; hydrogen atoms and minor occupied disordered atoms are omitted for clarity. Selected interatomic distances [Å] and angles [°]: Sb(1)–C(1) 2.157(1), Sb(1)–C(2) 2.238(1), Sb(1)–C(4) 2.217(2), P(1)–C(1) 1.860(1), P(1)–C(6) 1.891(1), P(1)–C(10) 1.886(1), Sb(1)...P(1) 3.306(1); C(1)–Sb(1)–C(2) 93.2(1), C(1)–Sb(1)–C(4) 91.3(1), C(4)–Sb(1)–C(2) 95.8(1), C(1)–P(1)–C(6) 100.2(1), C(1)–P(1)–C(10) 101.6(1), C(10)–P(1)–C(6) 111.3(1), P(1)–C(1)–Sb(1) 110.6(1).

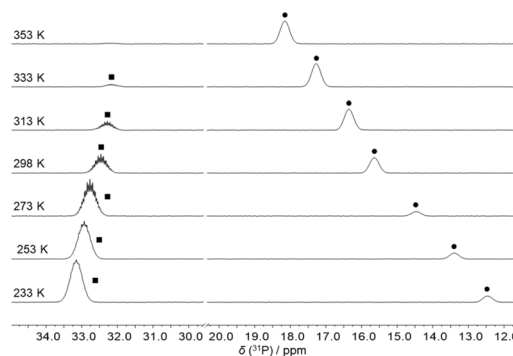


Fig. 2 ³¹P NMR spectra of a sample of a mixture of **1** and CS₂ at different temperatures. The peaks of the FLP **1** (●) and of the CS₂ adduct **2** (■) are labelled.

We performed Lewis acidity tests by the Gutmann–Beckett method²⁵ with OPET₃ and the modified method for soft Lewis acids with SePMe₃ presented by Lichtenberg.²⁶ After addition of OPET₃ to **1**, we did not see any variation in the chemical shifts of **1** and OPET₃. We assume that the antimony-oxygen interaction is too unfavourable. With the softer Lewis base SePMe₃, we observed a selenium transfer from SePMe₃ to **1** to give $(F_5C_2)_2SbCH_2(Se)P(tBu)_2$ and PMe₃.

Since these experimental Lewis acidity tests did not give a conclusive answer, we calculated the fluorine ion affinity (FIA) of **1** using a method by Greb *et al.* with an FIA of 278 kJ mol^{–1} it is well comparable to AsCl₃ (276 kJ mol^{–1}) and is below, for example, SbF₃ (290 kJ mol^{–1}), SbCl₃ (309 kJ mol^{–1}) and Sb(C₂F₅)₃ (315 kJ mol^{–1}).¹⁵

The reaction of FLP **1** with CO₂ gave no detectable adduct. In contrast, the reaction with CS₂ resulted in a temperature-dependent equilibrium, as observed by VT-NMR spectroscopy (Fig. 2). At room temperature, there is an equilibrium between the adduct **2** and the free FLP **1** plus free CS₂ in approximately equal proportions. After cooling the solution to 233 K, the adduct is dominant in the solution and only 10% of the free FLP remains unbound. Cooling the solution shifts the resonance of **1** ($\delta(^{31}P)$ at 298 K: 15.6 ppm) towards high field, while the multiplet of **2** ($\delta(^{31}P)$ at 298 K: 32.5 ppm) is low-field shifted.

This experimentally observed behaviour is confirmed by the results of Density Functional Theory (DFT) calculations (composite method r²SCAN-3c).²⁷ For the reaction of **1** with CS₂ to give the adduct **2** at room temperature, the change in free enthalpy is predicted to be very small: 4 kJ mol^{–1}.

The calculation predicts that the reaction is exergonic at 233 K ($\Delta G_{233 K} = -9$ kJ mol^{–1}). In contrast, when considering the conversion of **1** with CO₂, clearly positive values are calculated for both temperatures, 298 K ($\Delta G_{298 K} = 23$ kJ mol^{–1}) and 233 K ($\Delta G_{233 K} = 11$ kJ mol^{–1}). Even when the pressure is increased from 1 to 10 atm, the values for the two temperatures remain positive, although slightly lower ($\Delta G_{298 K} = 17$ kJ mol^{–1}; $\Delta G_{233 K} = 7$ kJ mol^{–1}). This theoretical prediction supports the experimental finding that **1** does not react with CO₂ to form a corresponding adduct.

The room temperature labile deep red crystals of **2** have been examined by X-ray diffraction. Unlike CS₂ adducts of



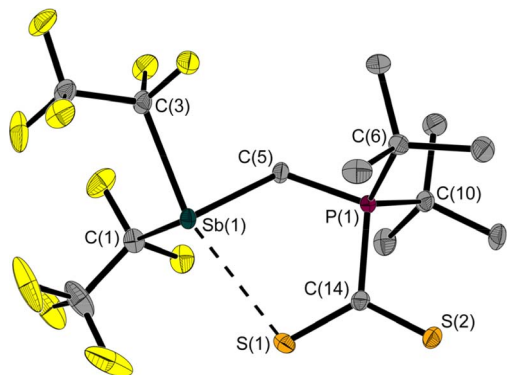


Fig. 3 Molecular structure of **2** in the solid state. Ellipsoids are set at 50% probability; hydrogen atoms are omitted for clarity. Selected interatomic distances [Å] and angles [°]: Sb(1)–C(1) 2.265(2), Sb(1)–C(3) 2.293(2), Sb(1)–C(5) 2.193(2), P(1)–C(5) 1.791(2), P(1)–C(6) 1.870(2), P(1)–C(10) 1.875(2), P(1)–C(14) 1.844(2), S(1)–C(14) 1.681(2), S(2)–C(14) 1.657(2), Sb(1)–S(1) 2.964(1); C(1)–Sb(1)–C(3) 91.1(1), C(5)–Sb(1)–C(1) 90.4(1), C(5)–Sb(1)–C(3) 85.9(1), C(5)–P(1)–C(14) 108.4(1), P(1)–C(5)–Sb(1) 115.2(1), S(1)–C(14)–P(1) 116.6(1), S(2)–C(14)–S(1) 127.1(1), S(2)–C(14)–P(1) 116.3(1), S(1)–Sb(1)–C(3) 160.8(1).

comparable FLPs,^{5,7} the structure of **2** is not that of a typical five-membered heterocycle (Fig. 3).

The Sb⋯S distance of 2.964(1) Å is intermediate between the sum of the *van der Waals* radii ($\Sigma r_{\text{vdW}}(\text{Sb}, \text{S}) = 3.86 \text{ Å}$)^{28,29} and the sum of the covalent radii ($\Sigma r_{\text{covalent}}(\text{Sb}, \text{S}) = 2.45 \text{ Å}$) with a tendency towards the latter. The attractive Sb⋯S interaction leads to a quasi-five-membered ring. The S(1)–Sb(1)–C(3) angle of 160.8(1)° identifies the Sb⋯S interaction as a weak pnictogen bond with a deviation from 180° expected for a σ -hole-type interaction. The P–C–Sb angle in **2** at 115.2(1)° is larger than in **1** at 110.6(1)°.

Another even weaker (intermolecular) interaction is between Sb(1) and S(2)' (symmetry: $1 - x, 1 - y, 1 - z$; Fig. S41†). The distance of 3.640(1) Å is slightly below the sum of the *van der Waals* radii ($\Sigma r_{\text{vdW}}(\text{Sb}, \text{S}) = 3.86 \text{ Å}$).^{28,29} This interaction presumably also contributes to the non-formation of a five-membered ring.

In order to better describe the interaction of the two heteroatoms Sb(1) and S(1), quantum chemical calculations were carried out. A Quantum Theory of Atoms in Molecules (QTAIM, PBE0/def2-TZVPP)³⁰ analysis gives a bond path for the Sb(1)⋯S(1) interaction with a not-so-small value for the charge density at the bond critical point (BCP) of $0.27e \text{ Å}^{-3}$ compared to the value of the Sb–C bond of $0.67e \text{ Å}^{-3}$ and other similar systems like Me₂Sb–SMe ($\rho_{\text{BCP}}(\text{Sb}–\text{S}) 0.61e \text{ Å}^{-3}$) or the adduct of the anthracene based, (F₅C₂)₂Sb–C≡C– substituted poly-Lewis acid with SMe₂ ($\rho_{\text{BCP}}(\text{Sb}–\text{S}) 0.11/0.16e \text{ Å}^{-3}$).¹⁷

This confirms the classification as half covalent, which is supported by the distance criterion. The corresponding Laplacian $\nabla^2 \rho_{\text{BCP}}(\text{Sb}–\text{S})$ has a small value of $0.96e \text{ Å}^{-5}$.

Based on the results of the QTAIM³⁰ and IQA (Interacting Quantum Molecules)³¹ analyses (Tables 1, S2,† Fig. 4), the interaction can be described as weakly stabilising, polar and partially covalent. For classification purposes we calculated reference systems, which are listed in the ESI.†

Table 1 Results of QTAIM³⁰ analyses for selected atom pairs in adducts **2** and **6**. Electron density at bond critical point, ρ_{BCP} [$e \text{ Å}^{-3}$], and Laplacian of the electron density at bond critical point, $\nabla^2 \rho_{\text{BCP}}$ [$e \text{ Å}^{-5}$]. Note that the numeration in the ESI is partly different. For more details, see the ESI

Compound	Atom pair A–B	ρ_{BCP}	$\nabla^2 \rho_{\text{BCP}}$
2	Sb(1)–S(1)	0.27	0.96
	Sb(1)–C(5)	0.67	1.69
	S(1)–C(14)	1.55	–9.64
6	Au(1)–P(1)	0.73	1.66
	Au(1)–P(2)	0.72	1.66
	Au(1)–Cl(1)	0.22	2.19
	Sb(1)–Cl(1)	0.19	1.20
	Sb(2)–Cl(1)	0.18	1.13

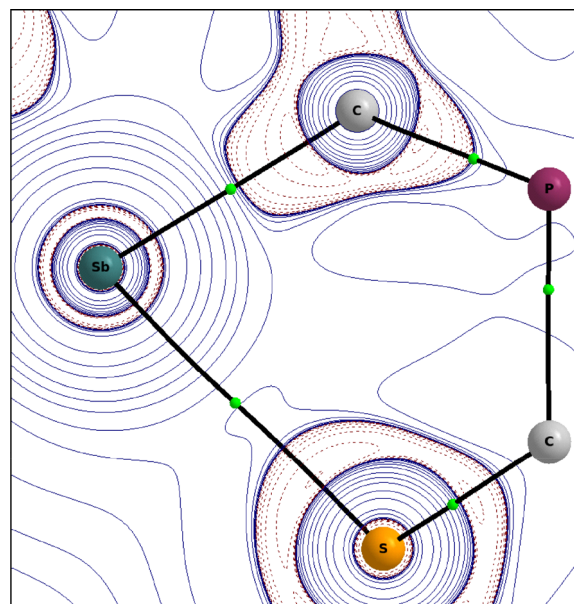


Fig. 4 Contour plot of the Laplacian $\nabla^2 \rho$ (positive isovalues are printed in full blue and negative ones as dashed red lines) of the electron density in the C(5)–Sb(1)–S(1) plane of **2**.

The interaction energy $E_{\text{int}}^{\text{AB}}$ of the atom pair Sb–S with $-8.20 \times 10^{-2} \text{ a.u.}$, lies between those of Li–F ($E_{\text{int}}^{\text{AB}} = -3.27 \times 10^{-1} \text{ a.u.}$) and Xe–Xe ($E_{\text{int}}^{\text{AB}} = -5.78 \times 10^{-3} \text{ a.u.}$) as reference values for typical ionic and typical dispersion interactions. As with the interaction in the dixonon molecule, the majority of the Sb–S interaction energy (84%) is due to electron exchange and correlation effects (see ESI† for more details).

In order to be able to make a statement about the influence of the Lewis acid on the reactivity of the phosphorus Lewis base towards CS₂ and the formation of a corresponding adduct, additional DFT calculations²⁷ were carried out. Due to the presence of the Lewis acid site in **1**, the reaction **1** + CS₂ → **1**·CS₂ ($\Delta H_{298\text{K}} = -53 \text{ kJ mol}^{-1}$) is significantly more exothermic than a comparable reaction of a phosphane of similar constitution around phosphorus, namely di-*tert*-butylmethylphosphane, with CS₂ ($\Delta H_{298\text{K}} = -13 \text{ kJ mol}^{-1}$).



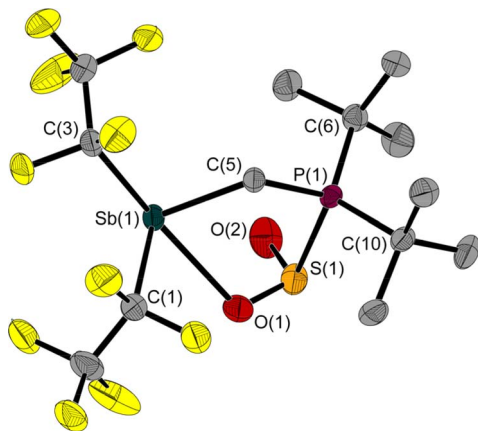


Fig. 5 Molecular structure of **3** in the solid state. Ellipsoids are set at 50% probability; hydrogen atoms and minor occupied disordered atoms are omitted for clarity. Selected bond lengths [Å] and angles [°]: Sb(1)–O(1) 2.483(2), Sb(1)–C(1) 2.242(3), Sb(1)–C(3) 2.281(3), Sb(1)–C(5) 2.199(2), S(1)–P(1) 2.285(1), S(1)–O(1) 1.498(2), S(1)–O(2) 1.470(2), P(1)–C(5) 1.803(2), P(1)–C(6) 1.852(3), P(1)–C(10) 1.857(2); C(1)–Sb(1)–O(1) 77.1(1), C(1)–Sb(1)–C(3) 87.7(1), C(3)–Sb(1)–O(1) 158.5(1), C(5)–Sb(1)–O(1) 78.0(1), C(5)–Sb(1)–C(1) 95.5(1), C(5)–Sb(1)–C(3) 88.6(1), O(1)–S(1)–P(1) 95.1(1), O(2)–S(1)–P(1) 102.8(1), O(2)–S(1)–O(1) 111.8(1), C(5)–P(1)–S(1) 104.3(1), S(1)–O(1)–Sb(1) 112.9(1), P(1)–C(5)–Sb(1) 114.9(1).

Although both reactions are endergonic, the reaction with *tert*-butylmethylphosphane, *i.e.* without the influence of a Lewis acid, is significantly more endergonic ($\Delta G_{298\text{ K}} = 36\text{ kJ mol}^{-1}$). The theoretical values thus indicate that the Sb \cdots S interaction, although weak, supports the adduct formation.

The reaction of **1** with SO₂ gives the adduct **3** with a five-membered heterocycle and an exocyclic S–O bond (Fig. 5). The angles around the sulphur atom add up to 309.7(3)°, describing distortion of the trigonal pyramidal coordination environment. The Sb atom is bisphenoidally surrounded with a C(3)–Sb(1)–O(1) angle of 158.5(1)° and a C(5)–Sb(1)–C(1) angle of 95.5(1)°.

Similar to **2**, the Sb(1)–C(5)–P(1) angle of 114.9(1)° in **3** is wider than in **1**. The ³¹P NMR chemical shift of **3** is 39.8 ppm, which is in a typical range for P atoms with a similar substitution pattern (*e.g.*: $\delta(^{31}\text{P})$ (F₅C₂)₃SnCH₂P(*t*Bu)₂·SO₂: 47.4 ppm⁵).

Surprisingly, the addition of phenyl isocyanate to **1** does not proceed *via* the C=O bond but *via* the C=N bond. This results in a five-membered heterocycle with exocyclic C=O and N–C_{ipso} bonds (Fig. 6).

However, in the light of the HSAB concept, this behaviour is to be expected: comparing the O and N atoms of the phenyl isocyanate, the latter is the softer one and should therefore be preferred to interact with the soft Sb atom. In **4**, the Sb(1)–C(5)–P(1) angle is also widened at 113.6(1)° compared to the free FLP **1**. In addition to the product signal set, the dissolved NMR sample contains a small proportion of the two reactants. IR spectroscopy was used to compare the isolated product as a solid and dissolved in CCl₄ with a solution of phenyl isocyanate in CCl₄. A band characteristic of phenyl isocyanate was detected in both solutions, but not in the solid sample. The isolated product **4** seems to decompose to a small extent into its reactants by dissolution.

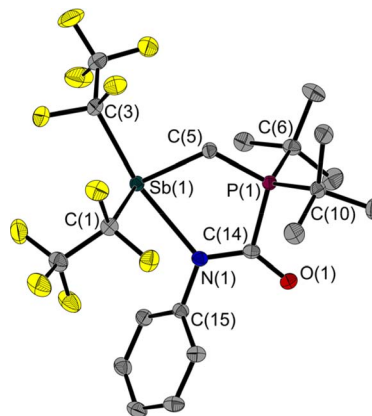


Fig. 6 Molecular structure of **4** in the solid state. Ellipsoids are set at 50% probability; hydrogen atoms are omitted for clarity. Selected bond lengths [Å] and angles [°]: Sb(1)–N(1) 2.473(1), Sb(1)–C(1) 2.253(1), Sb(1)–C(3) 2.332(1), Sb(1)–C(5) 2.180(1), P(1)–C(5) 1.792(1), P(1)–C(6) 1.856(1), P(1)–C(10) 1.852(1), P(1)–C(14) 1.860(1), O(1)–C(14) 1.243(2), N(1)–C(14) 1.322(2), N(1)–C(15) 1.428(2); C(1)–Sb(1)–N(1) 84.0(1), C(3)–Sb(1)–N(1) 159.7(1), C(5)–Sb(1)–N(1) 78.1(1), C(5)–P(1)–C(14) 108.0(1), C(14)–N(1)–Sb(1) 121.5(1), C(14)–N(1)–C(15) 117.7(1), C(15)–N(1)–Sb(1) 120.8(1), P(1)–C(5)–Sb(1) 113.6(1), O(1)–C(14)–P(1) 116.7(1), O(1)–C(14)–N(1) 132.0(1), N(1)–C(14)–P(1) 111.3(1).

In contrast to the addition of phenyl isocyanate described above, **1** reacts only to a small extent with phenyl isothiocyanate at the C=N but mainly at the C=S double bond (Fig. 7). The main product **5a** has a five-membered heterocycle, but in this case with an exocyclic C=N–Ph unit. This is consistent with the predictions of the HSAB concept. Compared to the other adducts presented here, the largest Sb(1)–C(5)–P(1) angle is found in **5a** with 119.3(1)°. The Sb(1)–S(1) bond with 2.881(1) Å is shorter than that in the CS₂ adduct **2**, and thus shorter than the sum of the *van der Waals* radii ($\Sigma r_{\text{vdw}}(\text{Sb}–\text{S}) = 3.86\text{ Å}$).^{28,29}

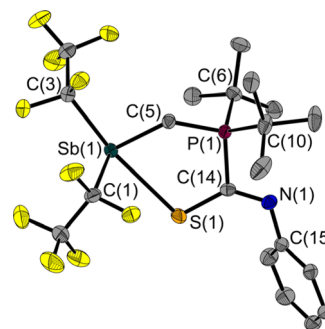


Fig. 7 Molecular structure of **5a** in the solid state. Only one of the two molecules in the asymmetric unit is shown. Ellipsoids are set at 50% probability; hydrogen atoms are omitted for clarity. Selected bond lengths [Å] and angles [°]: Sb(1)–S(1) 2.881(1), Sb(1)–C(1) 2.243(2), Sb(1)–C(3) 2.311(2), Sb(1)–C(5) 2.172(2), S(1)–C(14) 1.713(2), P(1)–C(5) 1.792(2), P(1)–C(6) 1.856(2), P(1)–C(10) 1.857(2), P(1)–C(14) 1.837(2), N(1)–C(14) 1.289(2), N(1)–C(15) 1.419(2); C(1)–Sb(1)–S(1) 86.1(1), C(3)–Sb(1)–S(1) 164.7(1), C(5)–Sb(1)–S(1) 80.1(1), C(14)–S(1)–Sb(1) 102.8(1), C(5)–P(1)–C(14) 109.4(1), C(14)–N(1)–C(15) 122.2(2), P(1)–C(5)–Sb(1) 119.3(1), S(1)–C(14)–P(1) 118.0(1), N(1)–C(14)–S(1) 131.8(1); N(1)–C(14)–P(1) 110.1(2).



Again, the Sb atom is bisphenoidally surrounded, with the C(3)–Sb(1)–S(1) angle of 164.7(1)° in the same range as in the previously discussed adducts.

Quantum chemical calculations (DFT)²⁷ on the different types of adduct formation behaviour are in agreement with the experimental results: the formation of the addition product to phenyl isocyanate **4** at the C=N bond is not significantly favoured in terms of energy (**4**: $\Delta G = -10 \text{ kJ mol}^{-1}$) compared to the addition at the C=O bond ($\Delta G = -6 \text{ kJ mol}^{-1}$). The same is true for the addition to phenyl isothiocyanate (**5a**: $\Delta G = -16 \text{ kJ mol}^{-1}$; C=N addition product **5b**: $\Delta G = -11 \text{ kJ mol}^{-1}$), so it is not surprising that addition to both sites is experimentally observed and not exclusively adduct **5a** is formed (Scheme 2). In the NMR spectra of the isolated solid of this reaction, there is a second set of signals with only slightly different chemical shifts, representing about a quarter of the mixture. The recorded data allow the following considerations: The connectivity of **5a** and the related tin compound, the adduct $(\text{F}_5\text{C}_2)_3\text{SnCH}_2\text{P}(\text{tBu})_2 \cdot \text{PhNCS}$, is analogous; consequently, there is a clear similarity in the chemical shifts of the respective isothiocyanate carbon atom and the *ipso* carbon atoms (Table 2). In contrast, **5b** shows larger deviations from the data of $(\text{F}_5\text{C}_2)_3\text{SnCH}_2\text{P}(\text{tBu})_2 \cdot \text{PhNCS}$.

We also analysed the adducts of phenyl isocyanate **4** and phenyl isothiocyanate **5a/5b** using two-dimensional NMR techniques (¹⁵N ¹H HMBIC).

The spectra contained signals of the free phenyl isocyanate or phenyl isothiocyanate, respectively, which were used as additional references for these samples. For both samples we observed only one other cross peak. These were very different from the chemical shifts of the reactants ($\delta(^{15}\text{N})$ of **4**: 150.3 ppm, $\delta(^{15}\text{N})$ of PhNCO: 48.4 ppm; $\delta(^{15}\text{N})$ of **5a**: 345.2 ppm, $\delta(^{15}\text{N})$ of PhNCS: 107.7 ppm) and also from each other; for **5b** we would expect a less significant deviation compared to **4**. Probably due to too low a concentration and a possible different relaxation behaviour, we could not detect a cross peak attributable to **5b**.

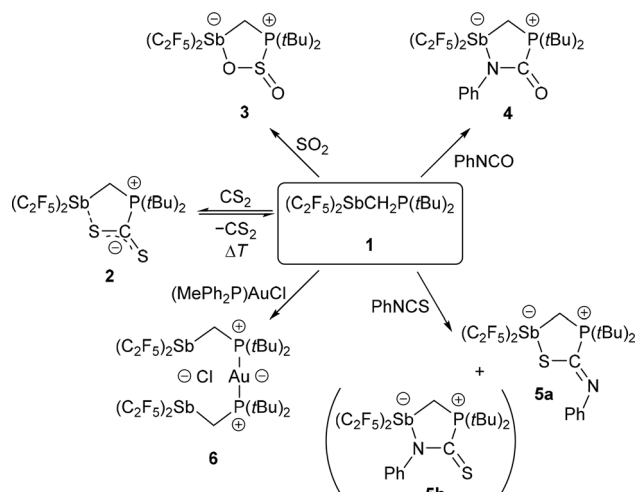
Table 2 Chemical shifts δ [ppm] of the PhNCE (E = O, S) and the *ipso* carbon atoms of the adducts of **1** with PhNCS and PhNCO and of $(\text{F}_5\text{C}_2)_3\text{SnCH}_2\text{P}(\text{tBu})_2$ with its respective adducts^{5,20}

Compound	$\delta(^{13}\text{C})$ PhNCE	$\delta(^{13}\text{C})$ C _{<i>ipso</i>}
1 ·PhNCS (5a)	168.7	151.0
1 ·PhNCS (5b)	178.2	147.3
1 ·PhNCO (4)	160.1	144.6
$(\text{F}_5\text{C}_2)_3\text{SnCH}_2\text{P}(\text{tBu})_2 \cdot \text{PhNCS}$	164.3	150.0
$(\text{F}_5\text{C}_2)_3\text{SnCH}_2\text{P}(\text{tBu})_2 \cdot \text{PhNCO}$	150.0	146.4

An attempt to assign the IR spectroscopic data of the adducts by using the results of quantum chemical calculations failed due to the lack of characteristic vibrational bands; a more precise identification of the constitutional isomers **5a** and **5b** is therefore not possible.

We note that a reference system for FLP **1** without Lewis acid function, namely MePtBu₂, shows no reactions with the substrates SO₂ and PhNCO, whereas it forms equilibria of adducts and precursors with CS₂ and PhNCS. The fact that all adducts of **1** are more stable than those of MePtBu₂ demonstrates that the antimony function in **1** (*i.e.* its FLP nature) is crucial for adduct formation with SO₂ and PhNCO and highly supportive for CS₂ and PhNCS.

In a reaction of **1** with the phosphane-gold chloride (MePh₂P)AuCl, two molecules of the free FLP reacted with one molecule of the gold compound, the MePPh₂ being displaced by the phosphane function of the FLP (Fig. 8). An almost linear coordinated gold atom is obtained; the P(1)–Au(1)–P(2) angle is 174.6(1)°, similar to other gold(i) complexes with two



Scheme 2 Reactions of FLP **1** with selected substrates at room temperature.

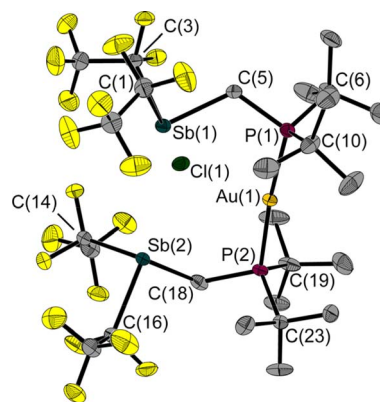


Fig. 8 Molecular structure of **6** in the solid state. Ellipsoids are set at 50% probability; hydrogen atoms and minor occupied disordered atoms are omitted for clarity. Selected bond lengths and interatomic distances [Å] and angles [°]: Au(1)–P(1) 2.311(1), Au(1)–P(2) 2.319(1), Sb(1)–C(1) 2.309(3), Sb(1)–C(3) 2.259(3), Sb(1)–C(5) 2.169(2), Sb(2)–C(14) 2.173(5), Sb(2)–C(16) 2.310(3), Sb(2)–C(18) 2.153(3), P(1)–C(5) 1.823(3), P(2)–C(18) 1.826(3), Au(1)···Cl(1) 2.939(1), Cl(1)···Sb(1) 2.966(1), Cl(1)···Sb(2) 2.981(1); P(1)–Au(1)–P(2) 174.6(1), C(3)–Sb(1)–C(1) 89.7(1), C(5)–Sb(1)–C(1) 93.3(1), C(5)–Sb(1)–C(3) 86.9(1), C(14)–Sb(2)–C(16) 89.8(1), C(18)–Sb(2)–C(16) 91.0(1), C(18)–Sb(2)–C(14) 107.1(2), C(5)–P(1)–Au(1) 112.7(1), C(18)–P(2)–Au(1) 113.7(1), P(1)–C(5)–Sb(1) 118.6(1), P(2)–C(18)–Sb(2) 117.8(1), Sb(1)···P(1)···P(2)···Sb(2) 4.8(1).



phosphane ligands.^{32,33} The distance between the gold and chlorine atom (2.939(1) Å) is greater than the sum of the corresponding covalence radii of 2.23 Å,²³ but well below the sum of the *van der Waals* radii of 3.41 Å,²⁹ indicating an attractive interaction between these two atoms. A distance shorter than the sum of the *van der Waals* radii is also found between the chlorine and the two antimony atoms (Cl(1)–Sb(1): 2.966(1) Å, Cl(1)–Sb(2): 2.981(1) Å, $\Sigma r_{vdW}(\text{Sb}–\text{Cl}) = 3.81$ Å).^{28,29} The Sb–C–P angles are 118.6(1)° and 117.8(1)°, which are wider than in the reactant **1**. For molecule **6**, we also performed QTAIM and IQA analyses (PBE0/def2-TZVPP) to describe the interaction of selected atom pairs (Tables 1 and S3†).^{30,31} Based on the calculations, the Au(1)–P(1/2) bonds are typically polarised bonds with a strong covalent character. In contrast the Au(1)–Cl(1) interaction can be considered as a weakly polarised bond with covalent character and a stabilisation energy about three times lower than that for Au(1)–P(1/2).

The interactions between the two antimony atoms and the chlorine atom are strongly stabilising, mainly ionic and have a stabilisation energy similar to that of the Au–P bonds. The calculations show that the P⋯Cl interactions are purely ionic and are even twice as strong as the Au(1)–Cl(1) interaction, despite the absence of bond critical points and bond paths. Also noteworthy is the presence of other low electron density bond paths for Cl⋯F and Cl⋯H (see ESI† for more details). The pronounced clamp-like structure is thus maintained not only in the solid state, but also likely to exist in the free molecules as predicted by quantum chemical optimisations. This seems to be due to the stabilising interactions between the FLP clamp and the chlorine atom.

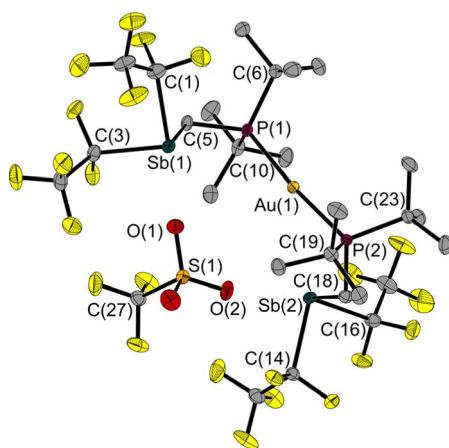


Fig. 9 Molecular structure of **7** in the solid state. Ellipsoids are set at 50% probability; hydrogen atoms are omitted for clarity. Selected bond lengths and interatomic distances [Å] and angles [°]: Au(1)–P(1) 2.328(1), Au(1)–P(2) 2.328(1), Sb(1)–C(1) 2.275(2), Sb(1)–C(3) 2.254(2), Sb(1)–C(5) 2.164(2), Sb(2)–C(14) 2.254(2), Sb(2)–C(16) 2.268(2), Sb(2)–C(18) 2.172(2), P(1)–C(5) 1.826(2), P(2)–C(18) 1.831(2), Au(1)⋯O(2) 3.521(2), O(1)⋯Sb(1) 2.647(2), O(2)⋯Sb(2) 2.808(2); P(1)–Au(1)–P(2) 173.9(1), C(3)–Sb(1)–C(1) 92.3(1), C(5)–Sb(1)–C(1) 91.8(1), C(5)–Sb(1)–C(3) 87.1(1), C(14)–Sb(2)–C(16) 89.8(1), C(18)–Sb(2)–C(16) 96.7(1), C(18)–Sb(2)–C(14) 87.6(1), C(5)–P(1)–Au(1) 116.8(1), C(18)–P(2)–Au(1) 111.7(1), P(1)–C(5)–Sb(1) 120.4(2), P(2)–C(18)–Sb(2) 115.8(2), Sb(1)⋯P(1)⋯P(2)⋯Sb(2) 111.1(1).

To see if this structural motif was also present without the chloride anion, we reacted compound **6** with silver triflate (AgOTf). By replacing the chloride anion with triflate, compound **7** was obtained as a colourless solid.

Its structure in the solid state shows no clamp-like shape (Fig. 9); the torsion angle (Sb–P–Sb) over the P axis is 106° wider than in **6**. The P(1)–Au(1)–P(2) angle of **6** (174.6(1)°) is almost identical to that of **7** (173.9(1)°).

The distance between the gold atom and the nearest oxygen atom of the triflate is 3.521(2) Å and thus exceeds the sum of the *van der Waals* radii ($\Sigma r_{vdW}(\text{Au}–\text{O}) = 3.18$ Å).²⁹ In turn, the distances between the antimony atoms and the nearest oxygen atoms of the anion fall below (O(1)–Sb(1): 2.647(2) Å, O(2)–Sb(2): 2.808(2) Å, $\Sigma r_{vdW}(\text{Sb}–\text{O}) = 3.58$ Å).^{27,28} The ³¹P NMR chemical shifts of the two gold adducts of this work ($\delta(^{31}\text{P})$ **6**: 74.0 ppm, **7**: 78.3 ppm) and the Sn FLP adduct ($\delta(^{31}\text{P})$ (F₅C₂)₃–SnCH₂P(*t*Bu)₂·AuCl(PPh₃) 74.4 ppm)⁵ are in a similar range.

Conclusions

We present here the neutral pre-organised Sb/P-Lewis pair (F₅C₂)₂SbCH₂P(*t*Bu)₂ (**1**) capable of forming the corresponding 1,2-addition products with various substrates, including CS₂, SO₂ and PhNCS, and the 2,3-addition product with PhNCO. The relatively soft acidic Sb(III)-Lewis function allows reversible binding of CS₂, whereas an adduct formation with CO₂ was not observed under similar conditions; an evaluation of the energy contributions to both reactions by quantum chemical calculations explains this experimental finding: the difference in free enthalpy for the formation of the CS₂ adduct at 298 K is 19 kJ mol^{−1} less than for the formation of the analogous CO₂ adduct and therefore its formation is much more favourable. These results are consistent with qualitative predictions from the HSAB concept. QTAIM and IQA analyses found a bond path with a bond critical point for the Sb–S interaction in the distorted five-membered ring adduct (F₅C₂)₂SbCH₂P(*t*Bu)₂·CS₂ and predicted its stabilisation energy to be -8.20×10^{-2} a.u.

For the adduct formation of the FLP with phenyl isocyanate and phenyl isothiocyanate, we found a preference for the adduct favoured by the HSAB concept, although the energetic difference between the different addition products is not significant. In the case of phenyl isothiocyanate both possible adducts are formed.

During adduct formation with (MePh₂P)AuCl, the phosphorus base of the gold moiety is displaced by a second FLP molecule, resulting in a stabilising clamp-like structure. Replacing the chloride anion with the larger triflate ion twists the FLP arms by 106° – another proof of the soft acid properties of **1**.

Data availability

The data published in this contribution are available as ESI, submitted with the manuscript. Crystallographic data have been deposited with the Cambridge Crystal Structure Database (CCDC).†



Author contributions

J. Krief: investigation, methodology, validation, visualization, writing (original draft), P. C. Trapp: investigation (DFT), Y. V. Vishnevskiy: investigation (QTAIM, IQA), B. Neumann: investigation (SCXRD), H.-G. Stammer: investigation (SCXRD), J.-H. Lamm: investigation (SCXRD), N. W. Mitzel: funding, acquisition, project administration, supervision, reviewing and editing.

Conflicts of interest

There are no conflicts to declare.

Acknowledgements

The authors thank Marco Wißbrock and Dr Andreas Mix for recording NMR spectra and Barbara Teichner for performing elemental analyses. This work was supported by Deutsche Forschungsgemeinschaft (grant MI 477/44-1, project number 461833739 and grant VI713/1-3, project no. 243500032). We furthermore thank the Regional Computing Center of the University of Cologne (RRZK) for providing computing time and support on the DFG-funded (Funding number: INST 216/512/1FUGG) HPC system CHEOPS.

References

- (a) D. W. Stephan, *Science*, 2016, **354**, aaf7229; (b) D. W. Stephan and G. Erker, *Angew. Chem., Int. Ed.*, 2015, **54**, 6400; (c) D. W. Stephan, *Dalton Trans.*, 2009, **17**, 3129.
- (a) G. C. Welch, R. R. San Juan, J. D. Masuda and D. W. Stephan, *Science*, 2006, **314**, 1124; (b) L. Keweloh, H. Klöcker, E.-U. Würthwein and W. Uhl, *Angew. Chem., Int. Ed.*, 2016, **55**, 3212; (c) A. F. G. Maier, S. Tussing, T. Schneider, U. Flörke, Z.-W. Qu, S. Grimme and J. Paradies, *Angew. Chem., Int. Ed.*, 2016, **55**, 12219; (d) C. M. Mömning, E. Otten, G. Kehr, R. Fröhlich, S. Grimme, D. W. Stephan and G. Erker, *Angew. Chem., Int. Ed.*, 2009, **48**, 6643; (e) E. Otten, R. C. Neu and D. W. Stephan, *J. Am. Chem. Soc.*, 2009, **131**, 9918.
- T. A. Kinder, R. Pior, S. Blomeyer, B. Neumann, H.-G. Stammer and N. W. Mitzel, *Chem.–Eur. J.*, 2019, **25**, 5899.
- B. Waerder, M. Pieper, L. A. Körte, T. A. Kinder, A. Mix, B. Neumann, H.-G. Stammer and N. W. Mitzel, *Angew. Chem., Int. Ed.*, 2015, **54**, 13416.
- P. Holtkamp, F. Friedrich, E. Stratmann, A. Mix, B. Neumann, H.-G. Stammer and N. W. Mitzel, *Angew. Chem., Int. Ed.*, 2019, **58**, 5114.
- (a) D. Zhu, Z.-W. Qu and D. W. Stephan, *Dalton Trans.*, 2020, **49**, 901; (b) E. A. Ilin, V. O. Smirnov, A. D. Volodin, A. A. Korlyukov and A. D. Dilman, *Chem. Commun.*, 2020, **56**, 7140; (c) L. Wickemeyer, N. Aders, A. Mix, B. Neumann, H.-G. Stammer, J. J. Cabrera-Trujillo, I. Fernández and N. W. Mitzel, *Chem. Sci.*, 2022, **13**, 8088; (d) C. Appelt, H. Westenberg, F. Bertini, A. W. Ehlers, J. C. Sloatweg, K. Lammertsma and W. Uhl, *Angew. Chem., Int. Ed.*, 2011, **50**, 3925; (e) C. Appelt, J. C. Sloatweg, K. Lammertsma and W. Uhl, *Angew. Chem., Int. Ed.*, 2013, **52**, 4256; (f) P. Federmann, T. Bosse, S. Wolff, B. Cula, C. Herwig and C. Limberg, *Chem. Commun.*, 2022, **58**, 1345.
- K. Samigullin, I. Georg, M. Bolte, H.-W. Lerner and M. Wagner, *Chem.–Eur. J.*, 2016, **22**, 3478.
- M. J. Gallagher, D. P. Graddon and A. R. Sheikh, *Thermochim. Acta*, 1978, **27**, 269.
- (a) G. A. Olah and R. H. Schlosberg, *J. Am. Chem. Soc.*, 1968, **90**, 2726; (b) G. A. Olah, G. Klopman and R. H. Schlosberg, *J. Am. Chem. Soc.*, 1969, **91**, 3261; (c) G. A. Olah, *J. Org. Chem.*, 2005, **70**, 2413; (d) L. Greb, *Chem.–Eur. J.*, 2018, **24**, 17881; (e) D. Tofan and F. P. Gabbaï, *Chem. Sci.*, 2016, **7**, 6768; (f) C.-H. Chen and F. P. Gabbaï, *Dalton Trans.*, 2018, **47**, 12075.
- M. Yang, D. Tofan, C.-H. Chen, K. M. Jack and F. P. Gabbaï, *Angew. Chem., Int. Ed.*, 2018, **57**, 13868.
- B. Pan and F. P. Gabbaï, *J. Am. Chem. Soc.*, 2014, **136**, 9564.
- (a) C.-H. Chen and F. P. Gabbaï, *Angew. Chem., Int. Ed.*, 2017, **56**, 1799; (b) G. Park and F. P. Gabbaï, *Chem. Sci.*, 2020, **11**, 10107; (c) Di You, B. Zhou, M. Hirai and F. P. Gabbaï, *Org. Biomol. Chem.*, 2021, **19**, 4949; (d) V. M. Gonzalez, G. Park, M. Yang and F. P. Gabbaï, *Dalton Trans.*, 2021, **50**, 17897.
- (a) J. S. Jones and F. P. Gabbaï, *Acc. Chem. Res.*, 2016, **49**, 857; (b) D. You, H. Yang, S. Sen and F. P. Gabbaï, *J. Am. Chem. Soc.*, 2018, **140**, 9644; (c) R. R. Rodrigues and F. P. Gabbaï, *Molecules*, 2021, **26**, 1985; (d) J. E. Smith, H. Yang and F. P. Gabbaï, *Organometallics*, 2021, **40**, 3886.
- D. Sharma, S. Balasubramaniam, S. Kumar, E. D. Jemmis and A. Venugopal, *Chem. Commun.*, 2021, **57**, 8889.
- (a) S. Benz, A. I. Poblador-Bahamonde, N. Low-Ders and S. Matile, *Angew. Chem., Int. Ed.*, 2018, **57**, 5408; (b) P. Erdmann, J. Leitner, J. Schwarz and L. Greb, *ChemPhysChem*, 2020, **21**, 987.
- (a) M. Yang, M. Hirai and F. P. Gabbaï, *Dalton Trans.*, 2019, **48**, 6685; (b) S. L. Benjamin, W. Levason, G. Reid and R. P. Warr, *Organometallics*, 2012, **31**, 1025; (c) K. Ohkata, S. Takemoto, M. Ohnishi and K. Akiba, *Tetrahedron Lett.*, 1989, **30**, 4841; (d) C. J. Carmalt, A. H. Cowley, R. D. Culp, R. A. Jones, S. Kamepalli and N. C. Norman, *Inorg. Chem.*, 1997, **36**, 2770; (e) A. M. Christianson and F. P. Gabbaï, *Organometallics*, 2017, **36**, 3013; (f) J. Qiu, B. Song, X. Li and A. F. Cozzolino, *Phys. Chem. Chem. Phys.*, 2017, **20**, 46; (g) M. Á. García-Monforte, M. Baya, D. Joven-Sancho, I. Ara, A. Martín and B. Menjón, *J. Organomet. Chem.*, 2019, **897**, 185.
- J. L. Beckmann, J. Krief, Y. V. Vishnevskiy, B. Neumann, H.-G. Stammer and N. W. Mitzel, *Angew. Chem., Int. Ed.*, 2023, **62**, e202310439.
- J. L. Beckmann, J. Krief, Y. V. Vishnevskiy, B. Neumann, H.-G. Stammer and N. W. Mitzel, *Chem. Sci.*, 2023, **14**, 13551.
- R. G. Pearson, *J. Am. Chem. Soc.*, 1963, **85**, 3533.
- P. Holtkamp, D. Poier, B. Neumann, H.-G. Stammer and N. W. Mitzel, *Chem.–Eur. J.*, 2021, **27**, 3793.
- (a) P. Holtkamp, J. Schwabedissen, B. Neumann, H.-G. Stammer, I. V. Koptuyug, V. V. Zhivonitko and



- N. W. Mitzel, *Chem.–Eur. J.*, 2020, **26**, 17381; (b) P. Holtkamp, T. Glodde, D. Poier, B. Neumann, H.-G. Stammler and N. W. Mitzel, *Angew. Chem., Int. Ed.*, 2020, **59**, 17388.
- 22 F. Eisenträger, A. Göthlich, I. Gruber, H. Heiss, C. A. Kiener, C. Krüger, J. U. Notheis, F. Rominger, G. Scherhag and M. Schultz, *New J. Chem.*, 2003, **27**, 540.
- 23 P. Pykkö and M. Atsumi, *Chemistry*, 2009, **15**, 186.
- 24 R. J. Gillespie and R. S. Nyholm, *Q. Rev. Chem. Soc.*, 1957, **61**, 339.
- 25 (a) M. A. Beckett, G. C. Strickland, J. R. Holland and K. S. Varma, *Polymer*, 1996, **37**, 4629–4631; (b) U. Mayer, V. Gutmann and W. Gerger, *Monatsh. Chem.*, 1975, **106**, 1235–1257.
- 26 J. Ramler and C. Lichtenberg, *Chem.–Eur. J.*, 2020, **26**, 10250–10258.
- 27 (a) S. Grimme, A. Hansen, S. Ehlert and J.-M. Mewes, *J. Chem. Phys.*, 2021, **154**, 064103; (b) J. W. Furness, A. D. Kaplan, J. Ning, J. P. Perdew and J. Sun, *J. Phys. Chem. Lett.*, 2020, **11**, 8208; (c) J. W. Furness, A. D. Kaplan, J. Ning, J. P. Perdew and J. Sun, *J. Phys. Chem. Lett.*, 2020, **11**, 9248; (d) S. Ehlert, U. Huniar, J. Ning, J. W. Furness, J. Sun, A. D. Kaplan, J. P. Perdew and J. G. Brandenburg, *J. Chem. Phys.*, 2021, **154**, 061101; (e) H. Kruse and S. Grimme, *J. Chem. Phys.*, 2012, **136**, 154101; (f) B. Metz, H. Stoll and M. Dolg, *J. Chem. Phys.*, 2000, **113**, 2563; (g) G. Herzberg, *Molecular Spectra and Molecular Structure. II. Infrared and Raman Spectra of Polyatomic Molecules*, Van Nostrand Comp., Toronto, 1945.
- 28 M. Mantina, A. C. Chamberlin, R. Valero, C. J. Cramer and D. G. Truhlar, *J. Phys. Chem. A*, 2009, **113**, 5806.
- 29 A. Bondi, *J. Phys. Chem.*, 1964, **68**, 441.
- 30 (a) R. F. W. Bader, *Atoms in Molecules - A Quantum Theory*, Oxford University Press, Oxford, 1990; (b) C. Adamo and V. Barone, *J. Chem. Phys.*, 1999, **110**, 6158; (c) F. Weigend and R. Ahlrichs, *Phys. Chem. Chem. Phys.*, 2005, **7**, 3297; (d) M. J. Frisch, G. W. Trucks, H. B. Schlegel, G. E. Scuseria, M. A. Robb, J. R. Cheeseman, G. Scalmani, V. Barone, G. A. Petersson, H. Nakatsuji, X. Li, M. Caricato, A. V. Marenich, J. Bloino, B. G. Janesko, R. Gomperts, B. Mennucci, H. P. Hratchian, J. V. Ortiz, A. F. Izmaylov, J. L. Sonnenberg, D. Williams-Young, F. Ding, F. Lipparini, F. Egidi, J. Goings, B. Peng, A. Petrone, T. Henderson, D. Ranasinghe, V. G. Zakrzewski, J. Gao, N. Rega, G. Zheng, W. Liang, M. Hada, M. Ehara, K. Toyota, R. Fukuda, J. Hasegawa, M. Ishida, T. Nakajima, Y. Honda, O. Kitao, H. Nakai, T. Vreven, K. Throssell, J. A. Montgomery Jr, J. E. Peralta, F. Ogliaro, M. J. Bearpark, J. J. Heyd, E. N. Brothers, K. N. Kudin, V. N. Staroverov, T. A. Keith, R. Kobayashi, J. Normand, K. Raghavachari, A. P. Rendell, J. C. Burant, S. S. Iyengar, J. Tomasi, M. Cossi, J. M. Millam, M. Klene, C. Adamo, R. Cammi, J. W. Ochterski, R. L. Martin, K. Morokuma, O. Farkas, J. B. Foresman and D. J. Fox, *Gaussian 16 Revision C.01*, Gaussian Inc. Wallingford CT, 2016.
- 31 M. A. Blanco, A. Martín Pendás and E. Francisco, *J. Chem. Theory Comput.*, 2005, **1**, 1096.
- 32 M. Barrow, H. B. Buergi, D. K. Johnson and L. M. Venanzi, *J. Am. Chem. Soc.*, 1976, **98**, 2356.
- 33 A.-M. Larssonneur, R. Turpin, P. Castan and G. Bernardinelli, *Inorg. Chim. Acta*, 1994, **227**, 85.

